PROCEEDINGS OF SCIENCE

Improving the photon sensitivity of the Pierre Auger Observatory with the AugerPrime Radio Detector

Jannis Pawlowsky[*a] **for the Pierre Auger Collaboration**[†b]

[a] *Bergische Universität Wuppertal,*
Gaußstraße 20, Wuppertal, Germany
[b] *Observatorio Pierre Auger,*
Av. San Martín Norte 304, 5613 Malargüe, Argentina

E-mail: spokespersons@auger.org

The AugerPrime upgrade represents a significant enhancement in the capability of the Pierre Auger Observatory to detect air showers. Central to this advancement is the installation of a radio antenna atop each existing Surface Detector station, constituting the Radio Detector (RD). The RD enhances the sensitivity of the Surface Detector to the electromagnetic component of air showers. Hence, the new detector presents an opportunity for the discovery of rare particles such as ultra-high-energy photons. This contribution shows the development efforts towards an RD trigger with focus on the detection of rare particles. The radio trigger designed for the detection of photon-induced events will be outlined, and the challenge of a radio background consisting of human-made noise is discussed. The trigger efficiency and reconstruction accuracy are studied with simulations. The presentation will conclude by summarizing the effectiveness of the new detector component.

10th International Workshop on Acoustic and Radio EeV Neutrino Detection Activities (ARENA2024)
11-14 June 2024
The Kavli Institute for Cosmological Physics, Chicago, IL, USA

[*]Speaker
[†]Full author list at http://www.auger.org/archive/authors_2024_08.html

PoS(ARENA2024)028

1. Introduction

The Pierre Auger Observatory in Argentina [1] aims to identify the sources of ultra-high-energy (UHE) particles. Through its measurements, alongside those from other observatories, it has compiled a list of potential sources of cosmic rays. However, the limited knowledge of galactic and extragalactic magnetic fields complicates narrowing the source list further down and introduces uncertainties when attempting to backtrack charged particles from Earth to their origins [2]. Detecting a single photon, on the other hand, would significantly advance our understanding of the origins of UHE particles. As non-charged particles, photons are not deflected in magnetic fields and would directly pinpoint their source location. The Pierre Auger Collaboration has performed various studies on UHE photons and has provided upper limits on the flux across a wide range of energies, e.g. [3]. The AugerPrime upgrade has the potential to make the first definitive UHE photon detection. The addition of the Radio Detector (RD) [4] to the baseline design improves the existing setup, providing optimal sensitivity to purely electromagnetic (EM) air showers in the atmosphere caused by UHE photons.

2. The AugerPrime Radio Detector - detecting EM air showers

The RD presents a substantial upgrade to the baseline design of the Pierre Auger Observatory. Consisting of a dual-polarised antenna, it is sensitive to the EM part of air showers. It complements perfectly the existing water-Cherenkov-detector (WCD) in the case of inclined air showers, as the WCD detects the incoming muons, while the EM particles are already absorbed in the atmosphere due to the large distance to the shower maximum. The radio emission in the sensitive frequency band of 30 MHz to 80 MHz can traverse these distances without being significantly absorbed, hence, recovering information about the EM component is possible.

The RD, mounted on top of the WCDs and having the regular Auger grid spacing of 1,500 m, is most efficient for high inclinations of the showers (e.g. zenith angles $\theta \in [65°, 85°]$). In this zenith angle range, the WCD becomes less efficient. Therefore, the RD enhances the mass sensitive range and increases the aperture for an assumed ideal efficiency by 1,611 km^2 sr (23 % of the Auger aperture) [5].

The benefits of the RD become best visible for air showers with low muon content and high EM contribution, such as those induced by ultra-high-energy photons. Detecting and accurately reconstructing these air showers is challenging: for vertical photon-induced events, the shower maximum can be well below ground. For inclined events, the muon content is often too low for triggering the WCD, while the EM component is already absorbed. Hence, the photon trigger efficiency becomes low, which is depicted in Fig 1 for inclined showers. It depends on mainly two parameters, the primary energy, E, and the zenith angle. For $E < 10$ EeV, the trigger efficiency is of the order of 5 % to 10 % for all zenith angles. At higher energies, the zenith angle range of $\theta \in [65°, 70°]$ shows the best trigger efficiency with approximately 70 %, while higher zenith angles have efficiencies below 25 %. Only for $E \geq 40$ EeV is almost full efficiency achieved for all zenith angles.

The RD can resolve the issue of decreased sensitivity to EM air showers for high inclinations. Not only can it detect the interesting inclined air showers with shower maxima well above ground

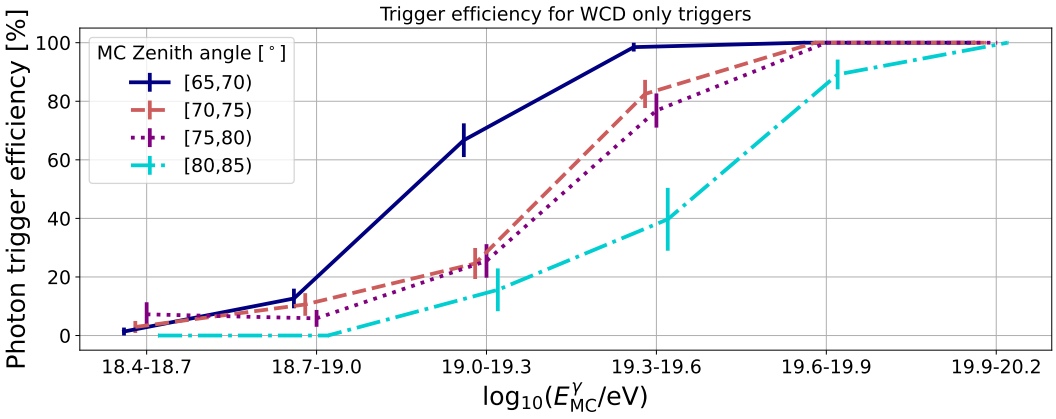

Figure 1: Photon trigger efficiency of the WCD detector for distinct primary energies. Different colours and line styles indicate the zenith angle range with a binning of 5°.

and with large distances to the shower maximum, but it draws its strength from it. Only for shower maxima distant from the detector is the radio emission fully developed and can be observed in multiple stations by the RD. Furthermore, the decreased sensitivity of the WCD now becomes a feature to discriminate the photon-induced showers from hadron-induced showers. Events with strong radio footprint, but weak particle signature on the ground point directly to an air shower induced by a neutral particle. As another feature, the RD adds direct access to the primary energy of the pure EM air showers of photons, which is challenging to reconstruct with the WCDs.

3. RD trigger design

Utilising the RD has many advantages for detecting photon air showers. However, it can only employ its full potential if a designated trigger is implemented, which makes the RD independent of the particle signature. The following trigger design is currently being tested, but so far, not deployed to the Auger array.

3.1 Radio threshold trigger

To trigger the read-out of the radio signal at the station-level, a classic threshold trigger is employed for the RD. The threshold, T_{H} (H for high, baseline-corrected and applied to the absolute value of the signal), is set, and peaks exceeding the threshold are registered. A station trigger is formed with the first bin exceeding T_{H} as the trigger time. This simple design was selected for various reasons. The trigger concept is a first implementation, which yields the most information about the morphology of triggers and resulting trigger rates. Learning from these properties, a more advanced algorithm could be employed. Potential advanced triggers are limited by the available resources on the FPGA of the RD. As an illustrative example, the threshold trigger is applied individually for each polarisation channel and each channel can create a trigger. A combination of both channels by e.g. the geometric sum is not possible due to missing free FPGA bits for the multiplication. Future improvements of the employed firmware could resolve this issue, but for a first implementation, a threshold trigger should suffice.

A threshold trigger is excellent for triggering on air showers. However, it is also vulnerable to triggering on noise. In particular, anthropogenic noise (RFI) can result in enormous trigger rates, hence, a vetoing mechanism is added to the threshold trigger. The vetoing algorithm is based on the distinct shapes of air shower signals and RFI noise. At Auger, air shower signals consist of short pulses with an almost uniform frequency distribution in the respective frequency band. No significant signal contribution is expected a few hundred nanoseconds after the signal maximum. In contrast, RFI is often of a single-frequency with persistent peaks over a relatively long time. Thus, simple peak-counting can be applied to differentiate between signal types. If more than $N_{\max}$ ($O(20)$) peaks exceed a second lower threshold, T_{L} (L for low, baseline-corrected and applied to the absolute value of the signal), in a search window positioned at a few hundred nanoseconds after the signal, the trigger is vetoed. The best values for $N_{\max}$, the window shift and the window length are subject to investigations.

The trigger and its vetoing mechanism are illustrated in Fig. 2. The left part shows a triggered air shower signal with clear signal peaks. No peak is exceeding T_{L} in the respective search window. The right side depicts RFI noise, which would not induce a trigger. Even though T_{H} is exceeded, too many peaks are detected with values above T_{L}. Hence, the trigger is rejected.

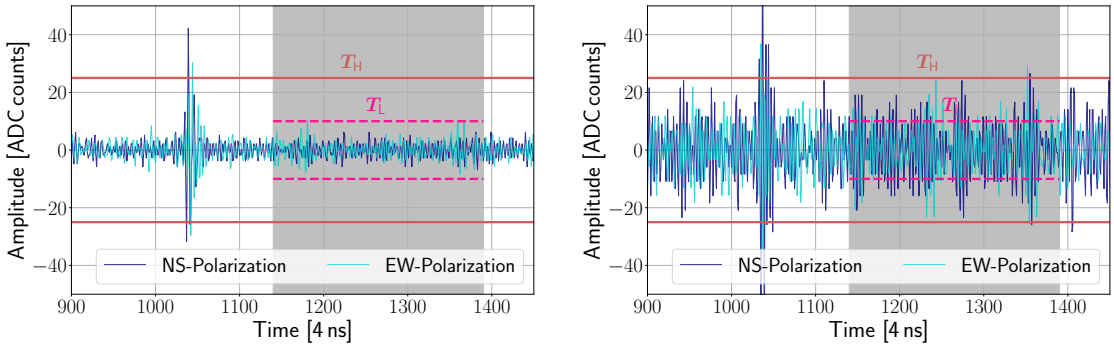

Figure 2: (Left) Accepted air shower signal triggered during a field test. The different blue lines indicate the polarization, the red solid lines show the applied trigger threshold. The grey area and magenta dashed lines indicate the settings of the vetoing mechanism. (Right) Illustration of a rejected trace with the same colour coding as (left).

3.2 Restrictions in the general trigger scheme

A strong rejection of noise is needed due to restrictions of the communication system of the Pierre Auger Observatory. The radio trigger is introduced to the regular trigger scheme of the Observatory, equivalent to the particle triggers of the WCD. Hence, the radio trigger also shares the available bandwidth with all other triggers, which is a substantial restriction. Each station has a bandwidth of 1,200 bits/s, which is used for sending of triggers and requested data. It limits the allowed average trigger rate to below 1 Hz with the additional requirement that the rate does not burst at any time. To prevent a bursting of radio triggers, the sending of triggers is inhibited for a time period of T_{inh} in the case that more than N_{inh} triggers are registered within one second.

The radio triggers are sent to the central data acquisition system (CDAS) [6], which decides whether the data is read-out. The triggers of the stations need to fulfill specific event building

requirements, which are detailed in reference [7]. The events can consist of purely WCD or RD triggers, or a mixture of both, and the minimal requirement for an event is to have at least three stations close to each other with coincident triggers. Subsequently, a read-out of the contributing stations is requested. Due to the limited communication bandwidth, data of fewer than ten events per station per day can be transferred.

4. Resulting aperture and sky coverage

The trigger design has been implemented in the Auger analysis framework, $\overline{\text{Off}}\underline{\text{line}}$ [8], and CoREAS simulations [9] (with CORSIKA 7.7410) have been employed. The simulation set consists of 1,700 photon-induced air showers with activated preshowering, $\log_{10}(E/\text{eV}) \in [18.4, 20.2]$ and $\theta \in [65°, 85°]$. The photon trigger efficiency is evaluated for different zenith angles and energies, using $T_{\text{H}} = 25$ ADC counts, which is a realistic value for an implementation, considering observed statistical noise fluctuations ($O(5-10)$ ADC counts). Combined with an aperture of Auger for the given zenith angle range of the RD, it results in the aperture with and without the radio trigger as depicted in Fig. 3. When implementing radio triggers, the largest increase in aperture is observed at low energies. For $\log_{10}(E/\text{eV}) \in [18.4, 18.7]$, the aperture is enhanced by a factor of 12, increasing from $\approx 50\,\text{km}^2\,\text{sr}$ to more than $600\,\text{km}^2\,\text{sr}$. The largest absolute increase is observed for $\log_{10}(E/\text{eV}) \in [18.7, 19]$, with a gain of almost $1{,}000\,\text{km}^2\,\text{sr}$. For higher energies, the difference diminishes, and both configurations converge towards the ideal aperture.

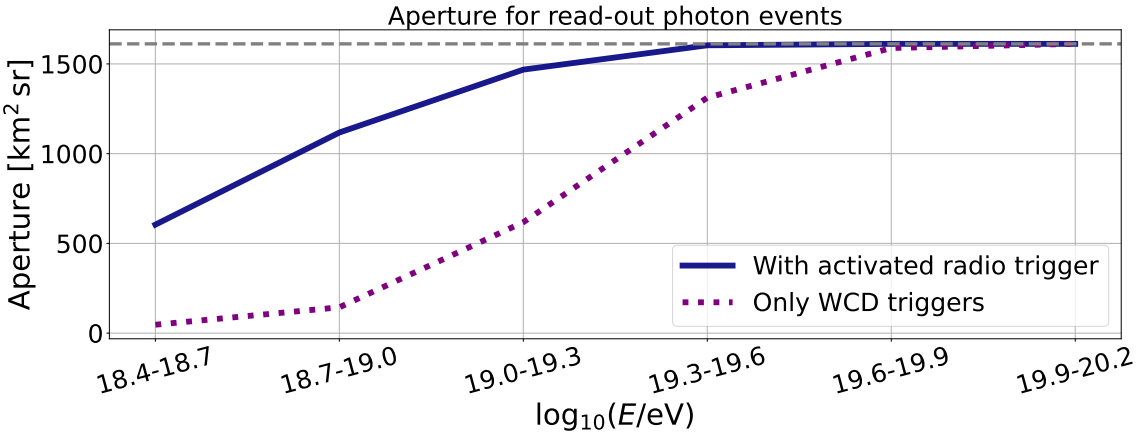

Figure 3: Aperture for different configurations of the triggering for distinct primary energies and a zenith angle range of $\theta \in [65°, 85°]$. Shown are the ideal aperture (grey dashed line), and the configurations with activated radio trigger (blue solid line) and only WCD triggers (purple dotted line).

The main contribution of the increased aperture is found in the zenith angle range of $\theta \in [70°, 80]$. Here, the trigger efficiency exceeds 50 % at the lowest energies, being almost fully efficient for $E \geq 10^{18.7}$ eV. Simultaneously, the zenith angle range yields a substantial ideal aperture. For $\theta \geq 80°$, a high trigger efficiency is observed as well, but it yields a small ideal aperture. For $\theta < 70°$, the trigger efficiency reaches full efficiency only at $E \geq 10^{19.3}$ eV.

Not only does the photon aperture increase with an implemented radio trigger, but also the sky coverage. A comparison of two zenith angle ranges, each 20° wide, is shown in Fig. 4 as an

exposure sky map. On the left, $\theta \in [40°, 60°]$ is depicted, a range often included in photon searches by Auger. It shows that most of the exposure is concentrated at one location and that a substantial fraction of 29 % of the sky is not covered. On the right, $\theta \in [65°, 85°]$ is illustrated, which shows that only 13 % of the sky is not covered. Moreover, the increased sky coverage enhances the overlap with Telescope Array, improving the possibility of joint searches and cross-calibrations.

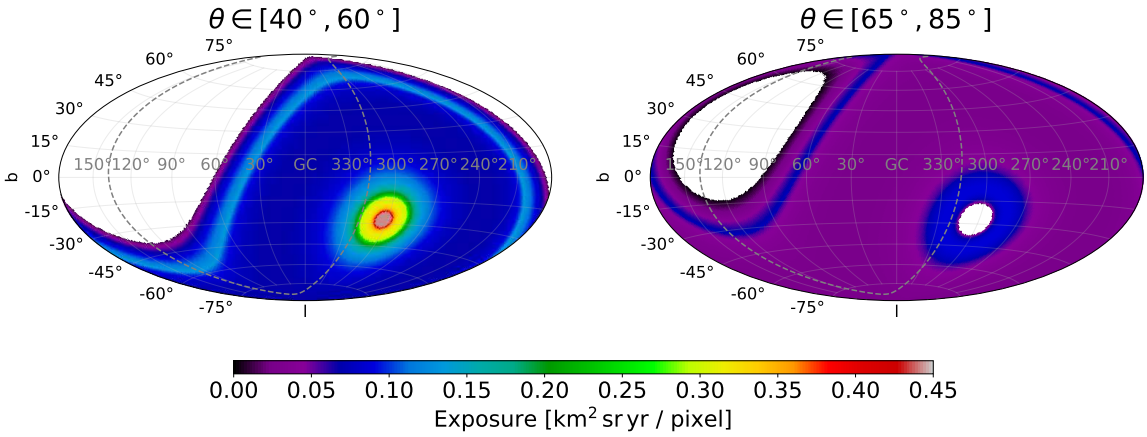

Figure 4: Sky maps in galactic coordinates for two different zenith angle ranges (Left: $\theta \in [40°, 60°]$, Right: $\theta \in [65°, 85°]$). The colour scale shows the exposure of Auger, while white areas indicate blind spots.

5. Field test

The proposed trigger design was employed in a field test. Two detector stations were selected, which makes event building from radio triggers impossible. The two stations with a spacing of 1.5 km are depicted in Fig. 5. With only two stations included in the test, CDAS is not stressed in the case of too many correlated radio triggers.

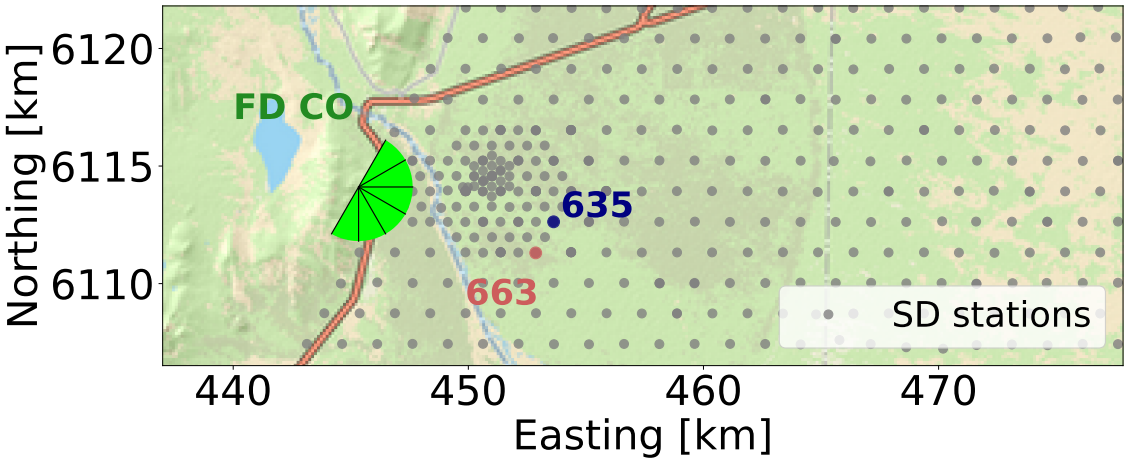

Figure 5: Map of the two stations (blue and red points) used in the trigger field test. The stations have a spacing of 1.5 km and are located at the edge of a denser station grid.

Table 1: Overview of the tested values for the trigger settings

Period	T_{H} [ADC counts]	T_{inh} [s]	N_{inh}
I	25	10	2
II	25	60	2
III	75	10	2
IV	50	10	1

The main purpose of the test was to determine the expected read-out rate of the trigger. A conservative estimation can be achieved by studying the correlation of the two stations. If they fulfil the event building coincidence criteria of trigger time differences less than 8 µs, we assume that the signal would have also reached a third station, resulting in an event*. The estimated rate is depicted in Fig. 6. It shows the number of expected read-outs per hour for the time of the test. Different settings of the trigger were tested, marked by periods **I** to **IV** and described in Tab. 1. All periods show an expected behaviour of bursting noise during consecutive hours. During daytime, anthropogenic noise sources are active, but they are quiet during the night. Hence, one has a recurring pattern of noisy and noise quiet periods. Significant differences can be seen between the periods. Period **I** shows bursts with maximum rates of nearly 100 read-outs/h. With stricter inhibit settings in period **II**, this is reduced to a maximum of ≈ 20 read-outs/h, while the loose settings in period **III** lead to the highest rates of 200 read-outs/h. At the end of period **III**, it suddenly becomes noise-quiet, nearly coinciding with the start of period **IV**. Only a few days into period **IV**, triggers are seen and read-outs would be expected, with maxima of the order of 10 read-outs/h. Two effects set in here, which are difficult to disentangle. First, at the end of period **III**, massive power cuts happened in the area of Auger. Therefore, ubiquitous noise sources were likely not active, and it took days for them to be reactivated. Second, period **IV** has the strictest settings of the trigger. It is unclear, if all noise sources were reactivated, or whether the strict settings led to the significantly reduced read-out rates.

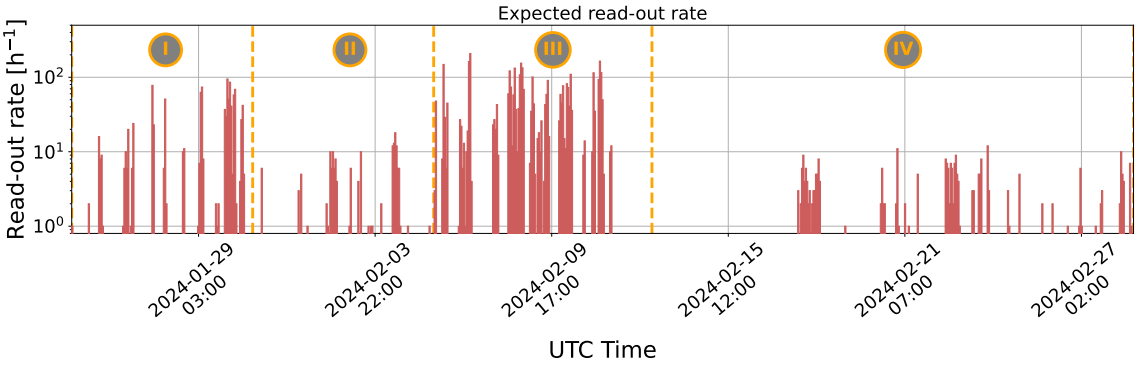

Figure 6: Expected read-out rate in case of deploying the radio trigger on a larger scale. The rates are calculated with the station triggers during the field test. Orange lines mark the beginning of different test periods with distinct trigger settings.

*There are good indications that the major fraction of events comes from a common signal and not from random coincidences of different signals.

All settings have in common that the expected read-out rates are significantly too high. The communication network cannot handle these amounts of data transfers. Hence, new ways have to be found to further reduce this trigger rate.

6. Future investigations

Three approaches are currently under investigation to suppress noise read-outs. The first one was already used in the trigger test. By not having pure radio events, the actual read-out rate was significantly reduced. This could be converted from a feature of the field test to a requirement in the event building. Pure radio events would not be allowed, and at least one particle trigger has to contribute. This reduces the read-out rate, but also lowers the photon trigger efficiency to $\approx 30\,\%$ instead of 60 % for pure radio events for $E \geq 10^{18.4}$ eV and $\theta \in [65°, 85°]$. Hence, it would be an intermediate step in order to study the morphology of triggers deeper.

A similar approach would reject pure radio events as well, but only those coming from the horizon. As anthropogenic noise sources are found on ground, noise is mostly originating from the horizon, where the phase space for events is minimal. Hence, one could reject most of the noise events while losing only a small fraction of air showers. However, this would require an online zenith angle reconstruction, based on station position and trigger times (with microsecond accuracy). Previous and ongoing studies indicate that the online zenith angle reconstruction is precise enough for this kind of rejection [10]. The rate of mis-reconstructed and therefore triggered noise is the next parameter to evaluate for this study.

Independent of the aforementioned approaches, the trigger design can be improved. Having more triggered traces due to the intermediate solutions, could help to enhance our understanding of noise and triggers, and would help to improve the trigger algorithm. Methods like triggering based on the SNR or rejections based on commonly known RFI frequencies are currently being studied.

In summary, the implementation of a radio trigger for the RD shows promising results, with the potential of increasing the aperture of the Observatory and enhancing the sky coverage for photon searches. First tests were successfully conducted, which increased our knowledge about noise sources and occurrences. Even though the ideal setting for the trigger to be bandwidth-compatible is yet to be found, a promising path is set for future photon searches.

References

[1] A. Aab et al. [Pierre Auger Collaboration], Nucl. Instrum. Meth. A 798 (2015), 172
[2] M. Erdmann et al., Astroparticle Physics 85 (2016), 54
[3] P. Abreu et al. [Pierre Auger Collaboration], JCAP 5 (2023), 21
[4] J. Hörandel for the Pierre Auger Collaboration, PoS(ARENA2024) (2024) 027
[5] T. Huege for the Pierre Auger Collaboration, EPJ Web Conf. 283 (2023) 06002
[6] R. Sato for the Pierre Auger Collaboration, PoS(ICRC2023) (2023) 373
[7] J. Abraham et al. [Pierre Auger Collaboration], Nucl. Instrum. Meth. A 613 (2010), 29
[8] S. Argirò et al. [Pierre Auger Collaboration], Nucl. Instrum. Meth. A 580 (2007), 1485
[9] T. Huege et al., AIP Conf. Proc. 1535 128 (2013)
[10] R. Uzeiroska, Bachelor thesis, 2021